

Regular and irregular features of classical motion described by a quadrupole boson Hamiltonian

V. Baran, A. A. Raduta, and D. S. Delion

Institute of Physics and Nuclear Engineering Bucharest, P.O. Box MG-6, Romania

(Received 21 December 1995; revised manuscript received 19 March 1996)

A fourth-order quadrupole boson Hamiltonian H is treated semiclassically through a time-dependent variational principle. The variational functions are coherent states for boson operators. In the parameters space of H there are regions, conventionally called “nuclear phases,” determining specific static properties. Several ground states corresponding to different equilibrium shapes are found as static solutions of classical equations of motion. The mechanism of destroying the tori of regular orbits and the onset of chaos depend on the nuclear phase. The regular and chaotic motions are analyzed in terms of Poincaré sections and the largest Lyapunov exponent. [S1063-651X(96)10309-3]

PACS number(s): 05.45.+b

I. INTRODUCTION

Many achievements of nuclear many-body formalisms such as the time-dependent Hartree-Fock formalism, the BCS treatment of the pairing interactions, the random-phase approximation (RPA), and boson expansion methods have a classical origin [1–9]. Indeed, the solutions for a stationary eigenvalue problem associated with an approximated many-body Hamiltonian can be obtained at the classical level by solving a set of time-dependent variational principle equations. Sometimes the quantal results obtained by some approximate procedures may be improved by the requantization of the classical motion. In general, results allowing for a correspondence of quantal and classical features have been a most attractive goal for physicists working in this field.

Alternatively, the nuclear structure and dynamics can be described by treating only a few degrees of freedom of collective character. Such a concept was introduced by Bohr and Mottelson [10] by quantizing the classical motion of the harmonic liquid drop (LD). Although the LD model is very successful in many conceptual respects, it is not able to describe the full picture for the quadrupole collective motion. Indeed, there are plenty of data whose interpretation is possible only by going beyond the harmonic picture. This stimulated alternative formalisms dealing with highly anharmonic terms in the model Hamiltonian. Here we enumerate only few of the attempts that contributed to a deeper understanding of nuclear structure in terms of boson degrees of freedom: the vibration-rotation (VR) model [11], the Greiner-Gneus model [12], the interacting boson approximation (IBA) [13], and the coherent state model (CSM) [14].

In contrast to the LD and VR models, which are classically motivated, some of these nuclear models, such as the IBA, are of quantum origin. This has led to explorations of the classical limits through a dequantisation procedure. For example, the classical limit [15] of the IBA model has been studied by several authors [16–23]. In this way it was possible to describe not only the static properties, corresponding to various symmetries, but also the excited states by quantizing the classical motion. Moreover, at the classical level, the connection between different quantal approaches [24] can be established. To give an example, the IBA model yields, in

the classical limit, the geometrical model [16,20,22,21].

In a previous paper [25] we initiated the study of classical properties of a fourth-order quadrupole boson Hamiltonian. We were interested in several aspects: (a) static features, (b) RPA-like equations for quadrupole intrinsic degrees of freedom, and (c) quantization of classical orbits. In another paper [26] we proved that the ground state and the two RPA one-phonon states are just the generating functions for the CSM formalism. In this way, the CSM acquires a classical foundation. Here we continue the project of the classical description of quadrupole degrees of freedom, pointing out possible relations of various classical “phases” (such as spherical, deformed, and γ unstable equilibrium shapes) and the onset of chaos. We address the question whether the onset of chaos carries any “fingerprint” of nuclear phases. Starting with an integrable limit, deviations leading to various phases are produced by an order parameter that in fact, decides to what extent the “order” and chaos share the phase space. The classical features generated by nonlinear dynamics are described in terms of Poincaré sections and the largest Lyapunov exponent [27–34]. Corresponding quantal aspects, such as Poisson versus Wigner distribution laws [35–39] for level energies statistics, are postponed to a future paper.

The article is outlined as follows. The model Hamiltonian is treated through a time-dependent variational principle formalism in Sec. II. Here we also describe the static properties as well as the RPA-like solutions of the classical equations of motion. The regular and chaotic orbits are analyzed in terms of Poincaré sections in Sec. III. A possible interpretation of the onset of chaos as being caused by an interfering effect of several resonances is presented. The maximal Lyapunov exponent is calculated for various nuclear “phases” as a function of classical energy and order parameters in Sec. IV. The final conclusions are drawn in Sec. V.

II. THE MODEL BOSON HAMILTONIAN AND ITS TDVP TREATMENT

Here we shall investigate some semiclassical features of a particular fourth-order quadrupole boson Hamiltonian

$$\begin{aligned}
H = & A_1[b^+b]_0 + \{A_2[b^+b^+]_0 \\
& + A_3([b^+b^+b^+]_0 + 3[b^+b^+b]_0) \\
& + A_4(\frac{1}{4}[b^+b^+]_0[b^+b^+]_0 \\
& + [b^+b^+]_0[b^+b]_0) + \text{H.c.}\} + A_4(\frac{1}{2}[b^+b^+]_0[bb]_0 \\
& + [b^+[b^+b]_0b]^0). \quad (2.1)
\end{aligned}$$

The quadrupole bosons are denoted by b_m^+ with $-2 \leq m \leq 2$. The coefficients A_m with $1 \leq m \leq 4$ are considered to be free parameters.

The Hamiltonian (2.1) differs from that used in a previous publication [25] in that Eq. (2.1) includes an additional term multiplied by A_2 . As shown later on, this term is necessary to approach γ unstable regimes. We study this Hamiltonian since it is the simplest fourth-order boson Hamiltonian (i.e., with a minimal number of parameters) that enables a full description of various nuclear equilibrium shapes. This assertion becomes obvious by writing H in terms of quadrupole shape coordinates α and their conjugate momenta π . This is done in the Appendix. From there one notes that H does not contain coordinate-momentum coupling terms. Also, the fourth-order terms in momenta are missing. Of course, the classical picture is changed if one takes another boson Hamiltonian. Also for a realistic description of nuclear spectra a more complex boson Hamiltonian is necessary. However, the simple structure of H suits the purpose of this work, i.e., to investigate the dependence of chaos onset on nuclear phases. Moreover, among parameters defining H , there is an order parameter B that describes the transition from order to chaos.

Some properties of H can be obtained by solving the equations of motion derived from a time-dependent variational principle (hereafter the units $\hbar = 1$ will be used)

$$\delta \int_0^t \left\langle \psi \left| H - i \frac{\partial}{\partial t'} \right| \psi \right\rangle dt' = 0. \quad (2.2)$$

If the variational states $|\psi\rangle$ span the whole boson space, solving Eq. (2.2) is equivalent to solving the time-dependent Schrödinger equation. Since this is not possible in practice, we chose as the variational function, the coherent state

$$|\psi\rangle = \exp[z_0 b_0^+ - z_0^* b_0 + z_2(b_2^+ + b_{-2}^+) - z_2^*(b_2 + b_{-2})] |0\rangle, \quad (2.3)$$

where $|0\rangle$ is the vacuum state for the quadrupole bosons and z_μ ($\mu=0,2$) are complex functions of time. The corresponding complex conjugate variables are denoted by z_μ^* . The set of functions z_μ, z_μ^* defines four-dimensional classical phase-space coordinates. The motivation for choosing such a trial function as well as the set of properties of H that might be described in this restricted space are given in Ref. [25]. The time-dependent treatment has the advantage, over the stationary ones, that besides the static properties, information about the dynamics of collective motion is obtained.

In order to fix the notations, the formalism of Ref. [25] will be reviewed briefly. In terms of the real u_μ and imaginary v_μ components of the phase-space coordinates

$$z_\mu = u_\mu + i v_\mu, \quad z_\mu^* = u_\mu - i v_\mu, \quad (2.4)$$

the equations of motions read

$$\begin{aligned}
\dot{u}_0 &= \frac{1}{2} \frac{\partial \mathcal{H}}{\partial v_0}, & \dot{v}_0 &= -\frac{1}{2} \frac{\partial \mathcal{H}}{\partial u_0}, \\
\dot{u}_2 &= \frac{1}{4} \frac{\partial \mathcal{H}}{\partial v_2}, & \dot{v}_2 &= -\frac{1}{4} \frac{\partial \mathcal{H}}{\partial u_2}, \quad (2.5)
\end{aligned}$$

where \mathcal{H} denotes the classical energy function defined as the expected value of H :

$$\begin{aligned}
\mathcal{H} \equiv \langle \psi | H | \psi \rangle = & A'(v_0^2 + 2v_2^2) + A(u_0^2 + 2u_2^2) \\
& + 2B u_0(6u_2^2 - u_0^2) + D(u_0^2 + 2u_2^2)^2. \quad (2.6)
\end{aligned}$$

The factors A, A', B, D are related to the coefficients A_m in the Hamiltonian H by the expressions

$$\begin{aligned}
A &= \frac{1}{\sqrt{5}}(A_1 + 2A_2), & A' &= \frac{1}{\sqrt{5}}(A_1 - 2A_2), & B &= \frac{16}{\sqrt{35}}A_3, \\
D &= \frac{5}{4}A_4. \quad (2.7)
\end{aligned}$$

It can be easily checked that the $2^{(2+\mu)/4}(u_\mu, v_\mu)$ with $\mu=0,2$ are canonically conjugate coordinates, i.e., their equations of motion are of Hamiltonian type, with $\sqrt{2}v_0$ and $2v_2$ taken as linear momenta.

The explicit form of Eqs. (2.5) are

$$\begin{aligned}
\dot{u}_0 &= A' v_0, \\
\dot{v}_0 &= -(A u_0 + 6B u_2^2 - 3B u_0^2 + 2D u_0^3 + 4D u_0 u_2^2), \\
\dot{u}_2 &= A' v_2, \\
\dot{v}_2 &= -(A u_2 + 6B u_0 u_2 + 4D u_2^3 + 2D u_0^2 u_2). \quad (2.8)
\end{aligned}$$

Note that \mathcal{H} is a constant of motion

$$\mathcal{H} = \text{const.} \quad (2.9)$$

Equation (2.9) defines the energy surface S of classical dynamics. Stationary points of the energy surface are particular solutions of Eqs. (2.5). Moreover, some of these are energy minima.

Equations (2.8) are highly nonlinear and therefore only numerical solutions are possible. However, trajectories lying close to a given minimum point might be reasonably well described by the linearized equations of motion, which are obtained by expanding the right-hand side of (2.8) around that point and retaining only the linear terms. The resulting equations are nothing else but the RPA equations for the intrinsic quadrupole boson degrees of freedom. The stationary points and RPA solutions are described in Secs. II A and II B, respectively, while the following subsection is devoted to some classes of exact numerical solutions.

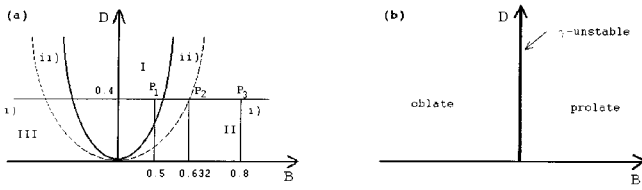


FIG. 1. (a) Parabola $D = \frac{9}{8}B^2$ (full line) and abscissa axis define three regions, in the upper plane $D \geq 0$, which are labeled as follows: I, in any point of this region, the potential energy has only one minimum that is spherical; II, there are two minima, one spherical and one deformed prolate; III, there are two minima, one spherical and one deformed oblate. Regions II and III are cut in two pieces by the parabola $D = B^2$ (dashed line): (i) The spherical minimum is higher than the deformed one. (ii) The spherical minimum is lower than the deformed one. (b) Phase diagram for $A = -A' = 1$. In the sector $D \geq 0, B > 0$ there are three prolate minima for the potential energy, while for $D \geq 0, B < 0$ the potential energy has three oblate minima.

A. Static solution

Without any loss of generality we can confine our considerations to the cases

$$|A| = A' = 1. \quad (2.10)$$

In what follows the two solutions of this equation are considered separately.

(1) The parameters A and A' are equal:

$$A' = A = 1. \quad (2.11)$$

If the remaining parameters B and D satisfy the equation

$$9B^2 - 8AD \leq 0, \quad (2.12)$$

the energy surface has only one stationary point and this is a minimum whose energy is equal to zero irrespective of values taken by B and D . The corresponding state describes a spherical shape. When the relation (2.12) is not obeyed, besides the spherical minimum, another six stationary points exist: three saddle points and three minima. Any of these six stationary points define a deformed shape. Classical states corresponding to these minima are degenerate. Saddle points are characterized by the same energy. These situations are synthesized in Fig. 1(a), where the parabola $D = \frac{9}{8}B^2$ and abscissa $D = 0$ determine three distinct phases: two deformed ones (II and III) and a spherical one (I). In region II, only prolate shapes appear, while in region III oblate shapes are obtainable.

The relative positions of spherical and deformed minima depend on $\text{sgn}(B^2 - D)$. Thus the parabola $D = \frac{9}{8}B^2$ determines two regions labeled (i) and (ii). In domain (i), the spherical minimum corresponds to an energy that is smaller than that determined by the deformed minimum, while in the region (ii) the two energies ordering is opposite. On the border $D = B^2$, the two minima are degenerate. In Fig. 2(a), for a fixed value of $u_2 (=0)$, the potential energies corresponding to the points P_1, P_2, P_3 specified in Fig. 1(a) are plotted as functions of u_0 , respectively.

(2) The parameters A' and A have opposite signs:

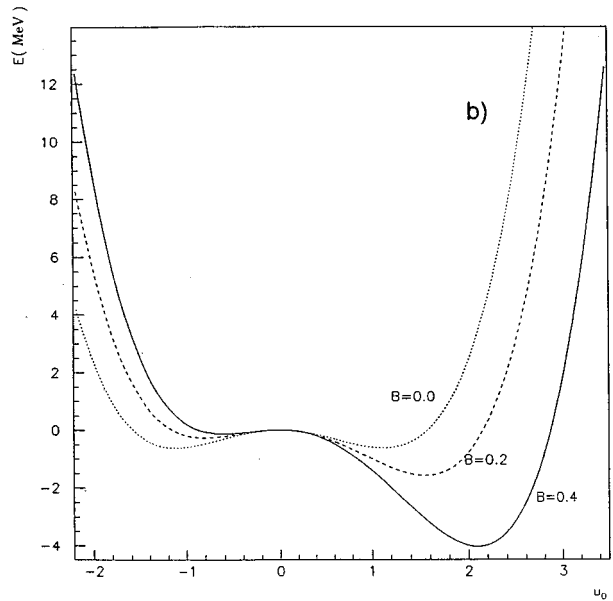
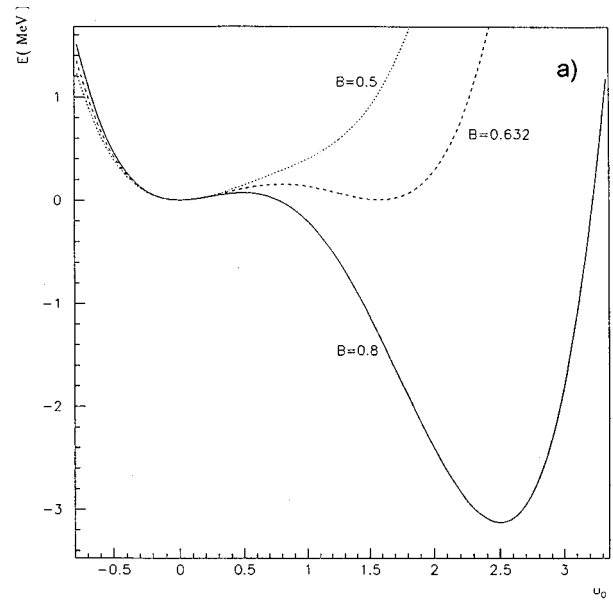


FIG. 2. (a) For $A = A' = 1$ a section $u_2 = 0$ of energy surface is plotted as a function of B . For $B = 0.5$ there is only one spherical minimum. For $B = 0.632$ there are two degenerate minima, while for $B = 0.8$ the deformed minimum is lower than the spherical one. (b) For $A = -A' = 1$ a section $u_2 = 0$ of energy surfaces is shown as a function of u_0 for three values of B . The right minima are also minima for the energy surface, while the left minima are saddle points for $B \neq 0$ and oblate minima for $B = 0$.

$$A' = -A = 1. \quad (2.13)$$

The phase diagram for this case is plotted in Fig. 1(b). When $B \neq 0$ there are seven stationary points: a maximum (the origin), three saddle points, and three deformed minima. For $B > 0$, the corresponding shapes are of prolate type, while for $B < 0$, the nuclear system exhibits an oblate shape. When $B = 0$, a γ -unstable regime is reached. Indeed, the classical energy has the ellipse

$$\beta^2 \equiv u_0^2 + 2u_2^2 = \frac{-A}{2D}, \quad (2.14)$$

as a continuous degenerate minimum. Here, like in Ref. 15, the following relation between phase space coordinates and nuclear deformations is used:

$$u_0 = \beta \cos \gamma, \quad u_2 = \frac{1}{\sqrt{2}} \beta \sin \gamma. \quad (2.15)$$

In Fig. 2(b) the energy surfaces, corresponding to three distinct values for the (D,B)-parameters, are sectioned by the plane $u_2=0$. The resulting curves have two minima and one maximum. It is worth noting that a γ unstable situation is characterized by a prolate-oblate shape coexistence. Moreover, the potential energy does not depend on γ . For $B \neq 0$, the left-hand side minima, shown in Fig. 2(b), are saddle points for the energy function.

B. The RPA treatment

The equations of motion (2.8) can be easily linearized by expanding their right-hand side around a deformed minimum. For the sake of simplicity, here we consider an axially deformed equilibrium shape described by the coordinate \hat{u}_0 . As shown in Ref. [25], the linearized equations have two solutions describing β - and γ -like oscillations. The corresponding energies have the expressions

$$\begin{aligned} \omega_0 &= [A'(A - 6B\hat{u}_0 + 6D\hat{u}_0^2)]^{1/2}, \\ \omega_2 &= [A'(A + 6B\hat{u}_0 + 2D^2)]^{1/2}. \end{aligned} \quad (2.16)$$

Taking into account the explicit expression of \hat{u}_0 [15], one finds a very simple equation for these energies:

$$\omega_2^2 - 3\omega_0^2 = 6AA'. \quad (2.17)$$

Hence, for γ stable nuclei, where $AA' > 1$, the following ordering equation holds:

$$\omega_2 > \omega_0. \quad (2.18)$$

When $AA' < 0$ and $B=0$, a γ unstable situation is reached. The potential energy does not depend on γ and therefore the “ γ oscillation” becomes spurious, which reflects, in fact, the existence of a constant of motion

$$\phi_\gamma = \text{const}, \quad (2.19)$$

with ϕ_γ the conjugate momentum of γ . Moreover, for

$$-AA' > \frac{\omega_0^2}{3}, \quad (2.20)$$

the ordering relation (2.18) is changed, i.e.,

$$\omega_2 < \omega_0. \quad (2.21)$$

III. REGULAR AND CHAOTIC FEATURES

In this section we shall analyze the classical trajectories satisfying the exact equations of motion (2.8). In the preceding section, two distinct classes of stationary points characterized by Eqs. (2.11) and (2.13) respectively, were considered. In both cases, the system is integrable if $B=0$. Indeed, there are two constants of motion: \mathcal{H} and ϕ_γ . By means of a

canonical transformation one can always choose two pairs of polar radii and angles as conjugate coordinates. Hence, such a system evolves on trajectories lying on a torus. These trajectories are conventionally called regular.

For $B=0$ it can be easily checked that up to a multiplicative constant the constant of motion (2.19) is given by

$$\phi_\gamma = \sqrt{2}(u_0 v_2 - u_2 v_0). \quad (3.1)$$

To what symmetry does this constant of motion correspond? To answer this question we note that the present procedure describes the intrinsic motion of the quadrupole degrees of freedom that span a two-dimensional space. Therefore, our problem is equivalent to that of two interacting oscillators system. The mapping of the boson operators onto the oscillator creation operators is achieved by

$$a_x^+ = b_0^+, \quad a_y^+ = \frac{b_2^+ + b_{-2}^+}{\sqrt{2}}. \quad (3.2)$$

Some time ago, a schematic model consisting of a two-dimensional oscillator potential plus a spin-orbit term, the mean field, and a special quadrupole-quadrupole interaction was proposed by Moszkowski in Ref. [40]. By varying continuously the relative strengths of spin-orbit and quadrupole-quadrupole interactions, the interplay between single-particle and collective features has been studied. Although the motion is taking place in a plane, this schematic model is able to simulate many predictions of realistic models. This is possible since the symmetry group is \mathfrak{R}_3 , describing rotations in a fictitious three-dimensional space and having

$$\begin{aligned} T_x &= \frac{1}{2}(a_x^+ a_x - a_y^+ a_y), \\ T_y &= \frac{1}{2}(a_x^+ a_y + a_y^+ a_x), \\ T_z &= \frac{1}{2i}(a_x^+ a_y - a_y^+ a_x) \end{aligned} \quad (3.3)$$

as generators. Since the classical Hamiltonian describes a planar motion, the \mathfrak{R}_3 group and its subgroups might be good candidates for investigating its symmetries. Indeed, it is worth noting that ϕ_γ is just the expected value of T_z :

$$\phi_\gamma = \langle \psi | T_z | \psi \rangle. \quad (3.4)$$

This reflects the fact that for $B=0$, the commutation relation

$$[H, T_z] = 0 \quad (3.5)$$

holds for the quantal system. Therefore the constant of motion ϕ_γ corresponds to the invariance of H to the rotation around z axis in a fictitious space.

For $B \neq 0$, the symmetry corresponding to the constant of motion ϕ_γ is broken and moreover there is no new symmetry replacing it. Consequently, the system becomes non-integrable. Such a system is moving on trajectories that are very sensitive to any small change of initial conditions. Because of that the motion may acquire a chaotic behavior. A good signature for regular and chaotic trajectories are their

intersections with the surface of Poincaré section defined as follows. Consider the system initial position at the point $P(u_0^{(i)}, v_0^{(i)} > 0, u_2^{(i)}, v_2^{(i)})$ with v_0 chosen positive and so that $P \in S$, where S is defined by (2.9). The equations of motion provide the solution for the classical orbit

$$u_0 = u_0(t), \quad v_0 = v_0(t), \quad u_2 = u_2(t), \quad v_2 = v_2(t). \quad (3.6)$$

We record the times

$$t_0 \leq t_1 \leq t_2 \leq \dots \leq \dots \quad (3.7)$$

when the conditions

$$u_0(t) = u_0^{(i)}, \quad v_0(t) \geq 0, \quad \mathcal{H} = E \quad (3.8)$$

are fulfilled. For $t = t_k$ the trajectory passes through the plane (u_2, v_2) at the point $P_k = (u_2(t_k), v_2(t_k))$. For a regular orbit, the P_k are distributed sequentially on a closed curve, while for a chaotic orbit, the points P_k fill densely and randomly a certain region of the plane.

Now let us first consider the case of $A = A' = 1$, $B = 0.8, D = 0.4$, and three energy surfaces corresponding to $E = 0.025, 0.05$, and 0.07 MeV. In all cases, the surface of section is defined by the restrictions

$$u_0 = 0, \quad v_0 > 0, \quad \mathcal{H} = E. \quad (3.9)$$

The results are plotted in Figs. 3(a)–3(c), respectively, for several initial conditions. The saddle point energy is $E_s = 0.075$ MeV. As shown in Fig. 3(a), when the energy value is far away from E_s the trajectories are regular. By contrast, when the energy approaches the saddle point value the chaos appears. The closer the energy is to the saddle point, the larger the volume of the phase space filled with chaotic orbits. This conclusion hinges on the comparison of Figs. 3(b) and 3(c). In each of the three situations mentioned above, the motion takes place around the *spherical minimum* of the energy surface.

Keeping the same parameters A, A', B, D as before, consider the motion in the potential well corresponding to the *deformed minimum* shown in Fig. 2(a). In Figs. 3(d) and 3(e) the Poincaré surface of section defined by

$$u_0 = 2.5, \quad v_0 > 0, \quad \mathcal{H} = E, \quad (3.10)$$

with $E = 0.0$ and 0.95 , respectively, is shown. When the value of E is smaller than that of the saddle point energy E_s , all trajectories are regular. For $E > E_s$ chaotic trajectories, surrounding several minima of the energy surface may appear. If $E > E_s$ and initial conditions are chosen so that the trajectory encircles only one minimum, the motion is still regular. Finally, we note that there are portions on the energy surface where a regular motion exists, irrespective of the value of E . This might suggest that even for the situation when $B \neq 0$ there exists a second constant of motion.

Note that when $B \neq 0$ the third-order boson term is activated and consequently a classical cubic term in coordinates appears. Moreover, the expression of this new term is identical to the cubic term appearing in the Hénon-Heiles Hamiltonian [41]. Therefore the answer to the question whether an additional constant of motion exists for $B \neq 0$ (already given

in Ref. [41]) is “no,” i.e., the system is not integrable. This suggests that the class of regular orbits defined by means of the Poincaré surface of sections is larger than that of orbits characterizing integrable systems.

To answer the question how the chaos settles in this case, we invoke here the arguments given in Ref. [31], where the transition from regular to chaotic regime is attributed to the Hamiltonian amplitude instability, which, in fact, is predicted by the Kolmogorov-Arnold-Moser theorem [42–44]. Indeed the $B = 0$ Hamiltonian may be expressed in terms of two action variables canonically related to the two constants of motion. The third-order term can be expressed as a Fourier series with the general term of the type $\cos(m\phi_1 + n\phi_2)$, where ϕ_1 and ϕ_2 are the angles conjugate to the two actions, respectively. Increasing the energy, several resonant terms depending on frequencies may appear and favor the distortion or even the destruction of some tori. In this case, the space that was previously occupied by tori is filled now randomly by chaotic trajectories.

Let us analyze now the behavior of the classical trajectories when $-A = A' = 1, B = 0.2$, and $D = 0.4$. The corresponding potential energy is that represented in Fig. 2(b) by the dashed line. From there it is obvious that such a situation is close to a γ unstable picture. The saddle point energy, for this case, is -0.27 MeV and the depth of the secondary well is -1.58 MeV. In Figs. 3(f), 3(g), and 3(h) the Poincaré surface of sections

$$v_0 \geq 0, \quad \mathcal{H} = E, \quad (3.11)$$

with $E = -0.3, 0.0$, and 1.0 MeV and $u_0 = 1.25, 0.0$, and 0.0 , respectively, are plotted. Note that below the saddle point [Fig. 3(f)], the classical motion is again regular. Above the saddle point, two effects are to be noted. One is the distortion of the tori and another one is the appearance of the chaotic motion. Moreover, the chaotic phase-space volume is an increasing function of energy.

Figure 3(a) indicates that trajectories associated with the motion around the spherical minimum of the surface energy encircle five stable periodic trajectories that prick the section plane in the fixed elliptic points of the Poincaré mapping. By contrast, for the case corresponding to the deformed minimum, according to the Fig. 3(d), a single elliptic point exists.

The situation described in Fig. 3(f), which deviates only slightly from a γ unstable picture, exhibits two elliptic points, each of them being surrounded by another three satellite-like elliptic points reflecting the presence of active resonating terms in the classical Hamiltonian. A common property of all Poincaré sections presented above consists of their invariance with respect to the transformation $(u_2, v_2) \rightarrow (-u_2, -v_2)$. Obviously this feature is inherited from the classical energy function \mathcal{H} . Although in Fig. 3(a) the unstable trajectories fill a phase-space volume equal to zero (within the computer errors) the curves' distortion reveals the incipient stage of a resonant structure for the nonintegrable system. From Fig. 3(b) one sees that the chaos is accompanied by two effects: (a) the decrease of the number of the regular orbits encircling the stable trajectories and (b) some satellite islands appearing in the vicinity of stable trajectories. These islands reflect the presence of high-order resonances. The fact that for some parameters and energy, order

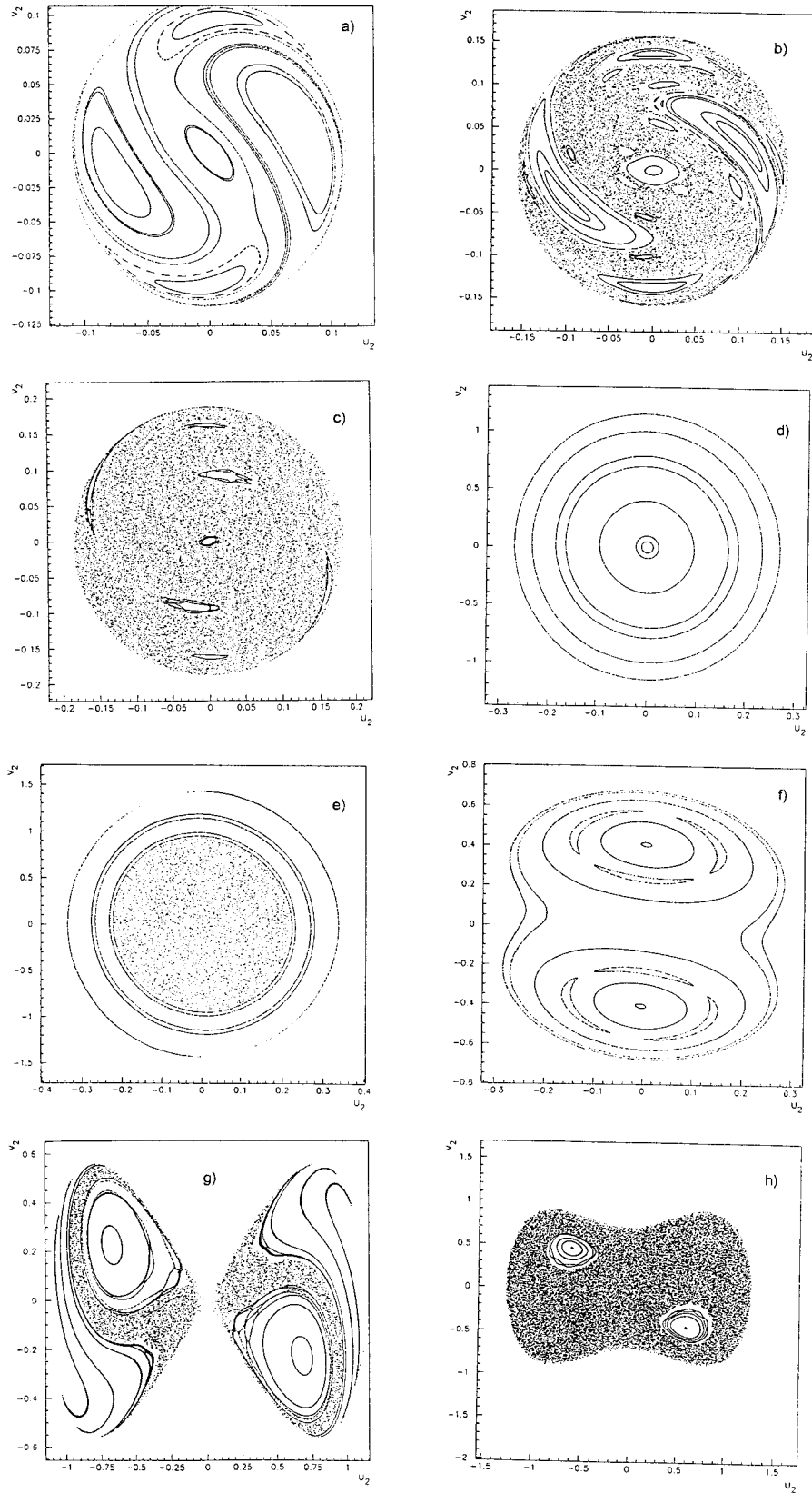


FIG. 3. (a) Poincaré surface section defined by the equations $u_0=0, v_0 \geq 0$, and $\mathcal{H}=0.025$ MeV. The parameters involved in the model Hamiltonian are $A=A'=1, B=0.8$, and $D=0.4$. (b) Poincaré surface section defined by the equations $u_0=0, v_0 \geq 0$, and $\mathcal{H}=0.05$ MeV. The Hamiltonian parameters are the same as in (a). (c) Poincaré surface section defined by $u_0=0, v_0 \geq 0$, and $\mathcal{H}=0.07$ MeV. The Hamiltonian parameters are the same as in (a). (d) Poincaré surface section defined by $u_0=2.5, v_0 \geq 0$, and $\mathcal{H}=0$. The Hamiltonian parameters are the same as in (a). (e) Same as in (d), but $\mathcal{H} = 0.95$ MeV. (f) Poincaré surface of section defined by $u_0=1.25, v_0 \geq 0$, and $\mathcal{H} = -0.3$ MeV. The Hamiltonian parameters were taken as $-A=A'=1, B=0.2$, and $D=0.4$ MeV. (g) Same as in (f), but $u_0=0$ and $\mathcal{H} = 0$ MeV. (h) Same as in (f), but $u_0=0$ and $\mathcal{H} = 1$ MeV.

and chaos share the phase space suggests that for the corresponding quantal system the energy spacings obey a law that is intermediary to the Poisson and Wigner distributions [38]. It is fair to say that the motion of our nuclear system around spherical, deformed, and γ unstable equilibrium shapes have Poincaré sections that are topologically distinct.

IV. LYAPUNOV EXPONENTS

In this section we study the orbits' character, regular or chaotic, from a different point of view, namely, by calculating the largest Lyapunov exponent, hereafter denoted by λ_{\max} . The regular orbits are characterized by $\lambda_{\max} \approx 0$, while $\lambda_{\max} > 0$ indicates a chaotic trajectory. The largest Lyapunov exponents for three phases—spherical, deformed prolate, and γ unstable—are presented and some specific features are pointed out. For an orbit surrounding the *spherical minimum* shown in Fig. 2(a), we plotted, in Fig. 4(a), the largest Lyapunov exponent as a function of energy (the value of the constant of motion \mathcal{H}) for two values of B . As we have already seen, this controls the transition between different phases (spherical deformed and γ unstable deformed). These values are $B=0.5$, for which the potential energy has only one minimum, and $B=0.632$, when the potential energy exhibits two minima. The remaining parameter D is taken to be equal to 0.4. To calculate λ_{\max} , the method described in Refs. [28, 30] was used.

One notes that λ_{\max} is an increasing function of B . This means that for a given energy, the larger B is, the larger the chaotic volume of phase space. It is worth noting that the slopes of the two functions, shown in Fig. 4(a), have a jump for an energy value equal to the saddle point energy E_s ($=0.075$ MeV). While for $E < E_s$, the slope is very large, indicating a rapid growth of chaos with energy, for $E > E_s$, λ_{\max} is slowly increasing with energy, suggesting that the chaos occupies almost the whole phase-space volume. In Figs. 5(a) and 5(b) for two values of excitation energy (with respect to the lowest minimum), the B dependence of λ_{\max} is studied. Three common features of these figures are to be mentioned. (i) For small values of B , λ_{\max} is small. Obviously this is a reminiscence of the $B=0$ case, when the system is integrable. At $B=0.2$ MeV the slope jumps to a larger value, showing a rapid development of the chaos, reaching a plateau at $B=0.44$ MeV that lasts until the value $B=0.59$ MeV. (ii) Starting with $B=0.59$ MeV [which marks the transition from the situation when the potential energy has only one (spherical) minimum to that with two minima (*one spherical and one deformed*)], the slope of λ_{\max} jumps to a larger value. (iii) The third common property is the discontinuity of the λ_{\max} for $B=0.8$. This indicates a transition from a chaotic to a regular regime and is caused by the fact the orbit is trapped by the well of the deformed minimum. This critical value of B is larger for larger values of excitation energy.

Now let us consider the case of $-A=A'=1$, which allows, by changing B , the study of the *prolate-oblate* transition through a γ unstable regime. In Figs. 4(b)–4(d) we plotted λ_{\max} as a function of energy, for three values of B . When B is large there is a tendency for a plateau that reflects a saturation effect indicating that the distance between the chosen orbits approaches the maximum value allowed by the

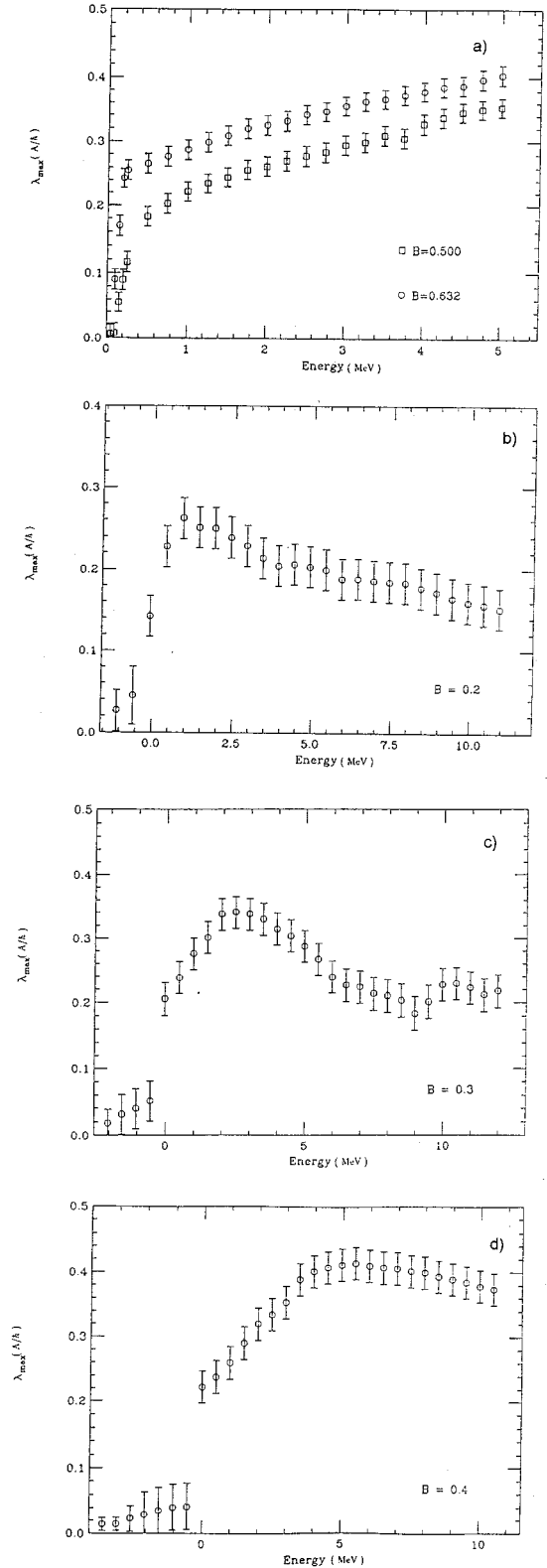


FIG. 4. (a) Largest Lyapunov exponent plotted as a function of classical energy, for two values of B . The parameter D is taken to be equal to 0.4, while A and A' are equal to 1. (b) λ_{\max} is plotted as a function of energy for a fixed set of parameters $-A=A'=1, B=0.2$, and $D=0.4$. (c) Same as in (b), but $B=0.3$. (d) Same as in (b), but $B=0.4$.

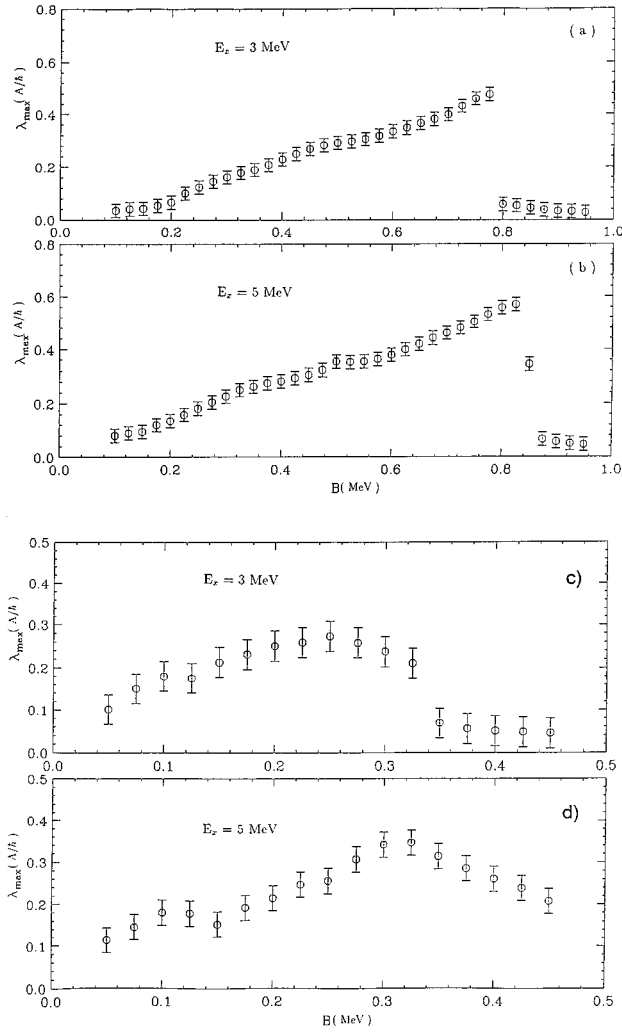


FIG. 5. Largest Lyapunov exponent plotted as a function of B for two values of the excitation energy: (a) $E_x=3$ MeV, and (b) $E_x=5$ MeV. The remaining parameters are the same as in Fig. 4(a). (c) λ_{\max} is plotted as a function of B for an excitation energy $E_x=3$ MeV. The coefficients of the model Hamiltonian are $-A=A'=1$, and $D=0.4$. (d) Same as in (c), but $E_x=5$ MeV.

finite size of the phase space. For two excitation energies, λ_{\max} is plotted versus B in Figs. 5(c) and 5(d). The largest Lyapunov exponent has a local minimum for $B=0.14$ and a global maximum in $B=0.25$ for $E_x=3$ MeV and $B=0.325$ for $E_x=5$ MeV. For $E_x=3$ MeV a sharp transition from a chaotic to a regular regime takes place at $B=0.325$. Such a transition is reached more slowly for $E_x=5$ MeV. Comparing Figs. 5(c) and 5(d) and Figs. 5(a) and 5(b), respectively, we note that in the former case the transition to the regular regime is reached for smaller value of B .

V. CONCLUSION

We have studied the classical static and dynamic features of a particular fourth-order boson Hamiltonian. The coupling of coordinates and momenta was ignored. Only kinetic energy terms that are quadratic in momenta are considered. The cases when the crossover term ($A_2=0$) and harmonic term ($A_1=0$) are missing were treated separately. These Hamiltonians allow for the description of various equilibrium

shape phase transitions such as spherical-prolate, spherical-oblate, and prolate-oblate via a γ unstable regime, respectively, by a smooth variation of an order parameter B (which multiplies the cubic term). We studied the onset of chaos for each of these phases. We found that for $B=0$, the system was integrable and therefore the classical motion is regular. Although the classical Hamiltonian contains fourth-order terms, an analytical solution for the second constant of motion (the first one being the energy) was possible. This corresponds to the symmetry expressing the classical Hamiltonian's invariance against rotations around an axis perpendicular to the plane (u_0, u_2) .

For $B \neq 0$ the chaos onset was studied in terms of Poincaré sections. The surface of section comprises the points of trajectories belonging to the plane (u_2, v_2) for a fixed value of u_0 and $v_0 \geq 0$. For every phase one finds a specific set of stable and periodic orbits encircled by tori of regular orbits. Also the resonances appearing in the amplitudes of the angle-dependent terms of the classical Hamiltonian, expressed as a function of action-angle pairs of conjugate variables, are different for different phases. Such resonances are accompanied by some tori destruction and chaos onset. The volume in the phase space that is governed by chaos depends on both the energy and order parameter B . For a given energy, the motion amplitude plays a decisive role in determining the character of the given orbit. To be more concrete, the trajectory is regular even for an energy larger than the saddle point energy if the initial conditions are so that the motion takes place around the deepest minimum. By contrast, if the orbit surrounds several energy surface minima, i.e., the motion amplitude is large, its chaotic character prevails. Global information about the distribution of the chaos and order in phase space given by the largest Lyapunov exponent was found to be consistent with our Poincaré sections.

Before closing, we would like to mention that a similar study in the IBA Hamiltonian was performed [32]. By contrast, our model Hamiltonian does not involve the s boson and does not conserve the number of bosons. If the terms of third order are missing, the system is integrable even though it contains high anharmonic terms, including some that do not commute with the boson number operator. In our case the order parameter is B (the strength of cubic terms), while for the IBA Hamiltonian, the parameter χ , the strength of the anharmonic quadrupole moment, dictates the transitions between different phases. While in Ref. [32] the analysis of chaos and order is confined to Lyapunov exponents, here we have also studied the Poincaré sections that give information about the local structure (chaos and order) of the phase space as well as about the dynamic of developing the chaos and destroying the order. In Ref. [32] the plot of Poincaré sections was not possible since the classical treatment accounts for all six degrees of freedom. However, by using a Monte Carlo procedure, the authors calculated the volume of the phase space occupied by chaos. A classical Hamiltonian depending on the β and γ nuclear deformations has been studied in Ref. [33], where their criterion for the onset of the chaotic motion was the negative curvature of the potential-energy surface. However, this only characterizes the local instabilities and is not suited for the behavior of trajectories surrounding two local minima. Finally, one may say that the

present paper provides a full picture of the competition between chaos and order for a nonintegrable system of two degrees of freedom that corresponds to a fourth-order quadrupole boson Hamiltonian describing the nuclear surface motion. These features are important for a realistic description of the coupling between surface fluctuations and other degrees of freedom in highly excited nuclei.

APPENDIX

In terms of quadrupole coordinates and conjugate momenta

$$\alpha_{\mu} = \frac{1}{\sqrt{2}} [b_{\mu}^{+} + (-)^{\mu} b_{-\mu}],$$

$$\pi_{\mu} = \frac{i}{\sqrt{2}} [(-1)^{\mu} b_{-\mu}^{+} - b_{\mu}], \quad -2 \leq \mu \leq 2, \quad (\text{A1})$$

the model Hamiltonian has the expression

$$H = A + B(\pi\pi)_0 + C(\alpha\alpha)_0 + D_3(\alpha\alpha\alpha)_0 + D_4(\alpha\alpha)_0(\alpha\alpha)_0. \quad (\text{A2})$$

The coefficients A, B, C, D_3, D_4 are related to those defining the boson Hamiltonian by

$$A = \frac{5}{2} \left(A_4 - \frac{1}{\sqrt{5}} A_1 \right), \quad B = \frac{1}{2} (A_1 - 2A_2),$$

$$C = \frac{1}{2} (A_1 + A_2) - \frac{7}{\sqrt{5}} A_4, \quad D_3 = 2\sqrt{2} A_3, \quad D_4 = A_4. \quad (\text{A3})$$

-
- [1] P. Kramer and M. Saraceno, *Geometry of the Time-Dependent Variational Principle in Quantum Mechanics*, Lecture Notes in Physics Vol. 140 (Springer, Berlin, 1981), p. 1.
- [2] K.-K. Kan, J.J. Griffin, and Z. Paltiel, Phys. Rev. C **21**, 1603 (1980).
- [3] J.P. Blaizot, Phys. Rev. B **107**, 331 (1981).
- [4] K. Goeke and P.G. Reinhard, Ann. Phys. **12**, 328 (1978).
- [5] J.P. Blaizot and Y. Orland, Phys. Rev. C **24**, 1740 (1981).
- [6] A. Klein, T. Marumori, and T. Une, Phys. Rev. C **29**, 246 (1984).
- [7] A. Kurriama and M. Yamamura, Prog. Theor. Phys. **71**, 973 (1984).
- [8] F. Sakata, T. Marumori, K. Muramatsu, and Y. Hashimoto, Prog. Theor. Phys. **74**, 51 (1985).
- [9] A.A. Raduta, V. Ceausescu, A. Gheorghe, and M. Popa, Nucl. Phys. A **427**, 1 (1984).
- [10] A. Bohr, Mat. Fys. Medd. Dan. Vid. Selsk. **26**, No. 14 (1952); A. Bohr and B. Mottelson, *ibid.* **27**, No. 16 (1953).
- [11] A. Faessler and W. Greiner, Z. Phys. **168**, 425 (1962); **170**, 105 (1962); **177**, 190 (1964).
- [12] G. Gneuss, U. Mosel, and W. Greiner, Phys. Lett. **30B**, 397 (1969).
- [13] A. Arima and F. Iachello, Ann. Phys. **99**, 253 (1976); **111**, 201 (1978); **115**, 325 (1978); Phys. Rev. Lett. **40**, 6 (1978); **40**, 385 (1978).
- [14] A. A. Raduta, V. Ceausescu, A. Gheorghe, and R. M. Dreizler, Phys. Lett. **99B**, 444 (1981); Nucl. Phys. A **381**, 253 (1982).
- [15] R. Gilmore, J. Math. Phys. **20**, 891 (1979).
- [16] A. E. L. Dieperink, O. Scholten, and F. Iachello, Phys. Rev. Lett. **44**, 1747 (1990).
- [17] O. S. van Roosmalen and A. E. K. Dieperink, Phys. Lett. **100B**, 293 (1981).
- [18] A. E. L. Dieperink, in *Collective Bands in Nuclei*, edited by D. Wilkinson (Pergamon, New York, 1983).
- [19] Yang Ya Tian and J. M. Irvine, J. Phys. G **9** 185 (1983).
- [20] M. Moshinsky, Nucl. Phys. A **338**, 156 (1980).
- [21] A. S. Assenbaum and A. Weguiny, Phys. Lett. **120B**, 256 (1983).
- [22] O. S. van Roosmalen, Ph.D. thesis, Groningen University, 1982 (unpublished).
- [23] F. Iachello and A. Arima, *The Interacting Boson Model* (Cambridge University Press, 1987), p. 102.
- [24] V. Paar, in *Interacting Bosons in Nuclear Physics*, edited by F. Iachello (Plenum, New York, 1978), p. 163.
- [25] A. A. Raduta, V. Baran, and D. S. Delion, Nucl. Phys. A **588**, 431 (1995).
- [26] D. S. Delion, A.A. Raduta, and V. Baran (unpublished).
- [27] M. Henon, in *Chaotic Behavior of Deterministic Systems*, 1981 Les Houches Lectures, edited by G. Iooss, R. H. G. Helleman, and R. Stora (North-Holland, Amsterdam, 1982), p. 53.
- [28] G. Benettin, L. Galgani, and J. M. Strelcyn, Phys. Rev. A **14**, 2338 (1976).
- [29] H. D. I. Abarbanel, R. Brown, and M. B. Kennel, J. Nonlin. Sci. **1**, 175 (1991).
- [30] W. H. Steeb and J. A. Louw, *Chaos and Quantum Chaos* (World Scientific, Singapore, 1986).
- [31] G. H. Walker and J. Ford, Phys. Rev. **188**, 416 (1969).
- [32] Y. Alhassid and N. Whelan, Phys. Rev. C **43** 2637 (1991).
- [33] Y. L. Bolotin, V. Y. Gonchar, and E. V. Inopin, Yad. Fiz. **45**, 350 (1987).
- [34] Wei-Min Zhang, Craig C. Martens, Da Hsuan Feng, and Jian-Min Yuan, Phys. Rev. Lett. **61**, 216 (1988).
- [35] H. A. Weidenmüller, in *Nuclear Structure 1985*, edited by R. A. Broglia, G. Hagemann, and B. Herskind (North-Holland, Amsterdam, 1985).
- [36] R. U. Haq, A. Pandey, and O. Bohigas, Phys. Rev. Lett. **48**, 1086 (1982).
- [37] A. Richter, Nucl. Phys. A **553**, 417c (1993).
- [38] J. Zakrzewski, K. Dupret, and D. Delande, Phys. Rev. Lett. **74**, 522 (1995).

- [39] B. V. Chirikov and D. L. Shepejyansky, Phys. Rev. Lett. **74**, 518 (1995).
- [40] S. A. Moszkowski, Phys. Rev. **110**, 403 (1958).
- [41] M. Henon and C. Heiles, Astron. J. **69**, 73 (1964).
- [42] A. N. Kolmogorov, Dokl. Akad. Nauk. SSSR **98**, 527 (1954).
- [43] V. I. Arnold, Russ. Math. Surveys **18**, 85 (1963).
- [44] J. Moser, Nachr. Akad. Wiss. Göttingen, Math. Phys. Kl. **1**, 1 (1962).